Structural Engineering and Mechanics, Vol. 50, No. 1 (2014) 19-36
DOI: http://dx.doi.org/10.12989/sem.2014.50.1.019

Krylov subspace-based model order reduction for Campbell diagram analysis of large-scale rotordynamic systems

Jeong Sam Han*

Department of Mechanical Design Engineering, Andong National University, Andong 760-749, Korea

(Received August 13, 2013, Revised January 15, 2014, Accepted January 31, 2014)

Abstract. This paper focuses on a model order reduction (MOR) for large-scale rotordynamic systems by using finite element discretization. Typical rotor-bearing systems consist of a rotor, built-on parts, and a support system. These systems require careful consideration in their dynamic analysis modeling because they include unsymmetrical stiffness, localized nonproportional damping, and frequency-dependent gyroscopic effects. Because of this complex geometry, the finite element model under consideration may have a very large number of degrees of freedom. Thus, the repeated dynamic analyses used to investigate the critical speeds, stability, and unbalanced response are computationally very expensive to complete within a practical design cycle. In this study, we demonstrate that a Krylov subspace-based MOR via moment matching significantly speeds up the rotordynamic analyses needed to check the whirling frequencies and critical speeds of large rotor systems. This approach is very efficient, because it is possible to repeat the dynamic simulation with the help of a reduced system by changing the operating rotational speed, which can be preserved as a parameter in the process of model reduction. Two examples of rotordynamic systems show that the suggested MOR provides a significant reduction in computational cost for a Campbell diagram analysis, while maintaining accuracy comparable to that of the original systems.

Keywords: Model order reduction; Krylov subspace; rotordynamics; Campbell diagram; damped eigenvalue analysis; whirling frequency; critical speed

1. Introduction

Typical rotor-bearing systems consist of a rotor, a bearing support system, and attached components such as disks, blades, fans, and couplings. Their rotordynamic modeling requires careful consideration because it usually includes cross-coupled unsymmetrical stiffness, localized nonproportional damping, and frequency-dependent gyroscopic effects (Wagner *et al*. 2010). The standard rotordynamic analysis of rotor-bearing systems includes the damped frequencies, critical speeds, stability, and unbalanced response (Nelson 2007). Modeling techniques that utilize the finite element (FE) method for the rotordynamics have progressed and changed since their first use in the 1970s. Because of the increasing geometric complexity of various rotor-bearing systems, the FE model can easily reach a high order of degrees of freedom (DOF), which makes it computationally very expensive. Thus, it is nearly impossible to complete repeated dynamic analyses for a rotor-bearing system within a practical design cycle in order to investigate the critical speeds, stability, and unbalanced response.

* Corresponding author, Professor, E-mail: jshan@anu.ac.kr

The published literature shows that existing model order reduction (MOR) methods are already in practical use for large-size dynamic problems with symmetric system matrices such as nonrotating structures (Antoulas *et al*. 2001, Han 2012, 2013). The common model reduction methods are Guyan reduction (Guyan 1965, Rouch *et al*. 1980), model reduction by modal analysis (Kim *et al*. 1986, Khulief *et al*. 1997, Wang *et al*. 1994a), component mode synthesis (CMS) (Craig *et al*. 1968, Glasgow *et al*. 1980, Wang *et al*. 1994b, 1995), and balanced truncation (Moore 1981, Wang *et al*. 1999, Casciati *et al*. 2014).

In the Guyan reduction method, the selection of master and slave DOFs is usually based on the user's experience and understanding of the mode shapes and key points of interest for loads, bearings, and point masses (Rouch *et al*. 1980). Note that, although the Guyan reduction scheme is commonly found throughout the literature, it is not generally effective at reducing systems for dynamic analyses (Wagner *et al*. 2010).

In the modal analysis method, modal coordinates are used to represent the system and decouple the dynamic system equations of motion. The modes to retain can be selected, up to the mode of interest, with twice the frequency of interest (Das *et al*. 2008) or by using a middle frequency range (Guyader 2009). A real modal analysis is commonly used because real undamped eigenvalues can easily be calculated from the **M** and **K** system matrices. On the other hand, a complex modal analysis uses a damping matrix, a gyroscopic matrix, or both these system matrices to yield complex conjugate pairs of eigenvectors that are calculated from the generalized eigenvalue problem in a state space representation; they are used for the system reduction. Kim and Lee (1986) presented a matrix reduction technique using the modal data of the isotropic undamped stationary parts to analyze rotor-bearing systems. In relation to the differences between real and complex modal analyses, Khulief and Mohiuddin (1997) studied a rotor-bearing system with anisotropic bearings and gyroscopics for dynamic analysis. They concluded that there is little difference between the accuracies when using real and complex modes for reducing simple beam finite element models, when comparing real reduced models to the complex natural frequencies of the full system, rather than a reduced system via complex modes.

In the CMS method, the selections of both interface DOFs, the discretization of the full system, and the modes to be retained for each subsystem are determined by the user and are similar to those of a modal analysis (Craig *et al*. 1968). However, several interface schemes such as the fixed interface, free-interface, and hybrid interface methods are used (Qu 2004, Shanmugam *et al*. 2006, Wang *et al*. 1994b). One disadvantage of CMS is that the final equations are normally coupled. However, this reduction does contain the full system dynamics from a modal analysis, and the modal representation is independent of the boundary and interface coordinates, which is useful for modeling nonlinear supports such as bearings (Glasgow *et al*. 1980). Wang and Kirkhope (1994b, 1995) suggested a CMS method for damped rotor systems and applied it to a complex system modeled with beam elements. However, they did not consider the gyroscopics.

In balanced truncation, the states or modes that are most observable and controllable are selected to form the reduced basis of the model on the basis of an error criterion such as the infinity norm, a frequency weighted infinity norm, or the energy in the state by the Hankel singular value, which expresses the amount of energy in each state (Moore 1981, Gugercin *et al*. 2004, Sawicki *et al*. 1997, Casciati *et al*. 2014). In a related study, Mohiuddin *et al.* (1998) applied the direct truncation balanced model reduction method to a complex rotor bearing system with gyroscopics, rotary inertia, and light damping for analysis and controller design. The authors presented the use of the singular perturbation balanced truncation scheme to alleviate the steady-state offset error common to balanced truncation.

Although these common model reduction methods have already been applied to rotordynamic systems, there is still a gap in the understanding and application to rotor-bearing systems. The application of these model reduction methods typically does not address the important properties inherent to rotor-bearing systems, such as the unsymmetrical stiffness, nonproportional damping, and frequency-dependent gyroscopic effects. In addition, the application examples found in the literature have small computational sizes, where MOR is not actually necessary for a rotordynamic analysis (Wagner *et al*. 2010). As Wagner *et al*. mentioned, no study has conducted a large-scale rotor dynamic analysis and shown the effects of various model reduction methods on the analysis.

In this study, we demonstrate that a Krylov subspace-based MOR (Rudnyi *et al*. 2006, Han 2012, 2013) via moment matching significantly speeds up the Campbell diagram analysis to check the whirling frequencies and critical speeds of large-scale rotordynamic systems. This approach is shown to be very efficient, because it is possible to repeat the rotordynamic simulation with the help of a reduced system by changing the operating rotational speed, which can be preserved as a parameter in the process of model reduction. The numerical results show very good agreement with the original systems. Two finite element models, a turbomolecular pump (TMP) and the Nelson and McVaugh rotor system, are used as numerical examples to demonstrate the accuracy and efficiency of this MOR method for rotordynamic analysis.

2. Theory

2.1 Campbell diagram analysis

A Campbell diagram is one of the most important and frequently used tools for understanding the dynamic behavior of a rotating-bearing system (Nelson 2007). In rotordynamics, the general dynamic equation to be solved can be described in a stationary reference frame as (Wagner *et al*. 2010, ANSYS 2011)

$$\mathbf{M}\ddot{\mathbf{x}}(t) + (\mathbf{C} + \mathbf{G})\dot{\mathbf{x}}(t) + (\mathbf{K} + \mathbf{B})\mathbf{x}(t) = \mathbf{F}(t) \tag{1}$$

or expressed in a more general form

$$\tilde{\mathbf{M}}\ddot{\mathbf{x}}(t) + \tilde{\mathbf{C}}\dot{\mathbf{x}}(t) + \tilde{\mathbf{K}}\mathbf{x}(t) = \mathbf{F}(t) \tag{2}$$

$$\tilde{\mathbf{M}} = \mathbf{M} \tag{3a}$$

$$\tilde{\mathbf{C}} = \mathbf{C} + \mathbf{G} \tag{3b}$$

$$\tilde{\mathbf{K}} = \mathbf{K} + \mathbf{B} \tag{3c}$$

where **M**, **C**, and $\mathbf{K} \in \Re^{N \times N}$ are the standard mass, damping, and stiffness matrices, respectively. The gyroscopic matrix **G** depends on the rotational velocity and acts as the major contributor in a rotordynamic analysis. This skew-symmetric gyroscopic matrix is derived from the kinetic energy that results from gyroscopic moments. The rotating damping matrix **B** also depends on the rotational velocity, and modifies the apparent stiffness of the structure. The vectors $\ddot{\mathbf{x}}(t)$, $\dot{\mathbf{x}}(t)$, and $\mathbf{x}(t)$ are the acceleration, velocity, and displacement response vectors, respectively, and have dimension *N*. $\mathbf{F}(t)$ is the vector of the applied forces.

Mathematically, the Campbell diagram analysis requires several quadratic eigenvalue analyses with multiple steps corresponding to different values of rotational velocity, Ω. Provided that $\mathbf{F}(t) = \mathbf{0}$ in Eq. (2), the free vibration of the damped second-order system has a solution in the form (Qu 2004)

$$\mathbf{x}(t) = \boldsymbol{\psi} e^{\lambda t} \tag{4a}$$

and its first and second time derivatives are

$$\dot{\mathbf{x}}(t) = \lambda \boldsymbol{\psi} e^{\lambda t} \tag{4b}$$

$$\ddot{\mathbf{x}}(t) = \lambda^2 \boldsymbol{\psi} e^{\lambda t} \tag{4c}$$

where $\boldsymbol{\psi}$ is the N-dimensional vector of the amplitudes, and λ is the complex frequency of the response. Substituting the solution and its first and second time derivatives to Eq. (2) gives the following quadratic eigenvalue problem (QEP):

$$(\lambda^2 \tilde{\mathbf{M}} + \lambda \tilde{\mathbf{C}} + \tilde{\mathbf{K}}) \boldsymbol{\psi} = \mathbf{0} \tag{5}$$

In general, the eigenvalues are a function of the rotating velocity Ω, and the ith complex frequency has the general form $\lambda_i = \sigma_i + j\omega_i$. The real part of the eigenvalue, σ_i, is the damping constant, and the mode is unstable if it has a positive value. The imaginary part, ω_i, is the damped circular frequency of whirling in the rotordynamics. From the complex eigenvalues, we can determine the damped critical speed and the onset of speed instability.

Because it is quite difficult to solve Eq. (5) in the displacement space, the commonly used scheme for solving QEP is to transform Eq. (2) from the displacement space into the state space. We can introduce a supplemental identity equation as follows:

$$\mathbf{I}\dot{\mathbf{x}} - \mathbf{I}\dot{\mathbf{x}} = \mathbf{0} \tag{6}$$

Then, the free vibration of the damped system from Eq. (2) can be rewritten in the state space form as

$$\underbrace{\begin{bmatrix} \mathbf{I} & \mathbf{0} \\ \mathbf{0} & \tilde{\mathbf{M}} \end{bmatrix}}_{\mathbf{E}} \underbrace{\begin{Bmatrix} \dot{\mathbf{x}} \\ \ddot{\mathbf{x}} \end{Bmatrix}}_{\dot{\mathbf{y}}} + \underbrace{\begin{bmatrix} \mathbf{0} & -\mathbf{I} \\ \tilde{\mathbf{K}} & \tilde{\mathbf{C}} \end{bmatrix}}_{\mathbf{A}} \underbrace{\begin{Bmatrix} \mathbf{x} \\ \dot{\mathbf{x}} \end{Bmatrix}}_{\mathbf{y}} = \mathbf{0} \tag{7}$$

A $2N$-dimensional vector $\mathbf{y}$ defined as

$$\mathbf{y} = \begin{Bmatrix} \mathbf{x} \\ \dot{\mathbf{x}} \end{Bmatrix} \tag{8}$$

is referred to as the state vector because it includes both the displacement and velocity, and it

completely represents the state of the system. Using the state vector, the QEP given in Eq. (5) is transformed into the following first-order eigenvalue problem:

$$(\lambda \mathbf{E} + \mathbf{A})\boldsymbol{\eta} = \mathbf{0} \tag{9}$$

in which

$$\boldsymbol{\eta} = \begin{Bmatrix} \boldsymbol{\psi} \\ \lambda \boldsymbol{\psi} \end{Bmatrix} \tag{10}$$

The $2N \times 2N$ matrices **E** and **A** are real but indefinite and unsymmetrical in general. This formulation doubles the size of the system matrices and thus increases the computational cost. When the FE model has a very large number of DOFs, it is often necessary to use MOR techniques to solve Eq. (7).

2.2 Krylov subspace-based MOR

The basic concept of the Krylov subspace-based MOR is to find a low-dimensional subspace $\mathbf{V} \in \Re^{N \times n}$ of

$$\mathbf{x} \cong \mathbf{V}\mathbf{z} \quad \text{where } \mathbf{z} \in \Re^n, \ n << N \tag{11}$$

so that the trajectory of the original high-dimensional state vector **x** in Eq. (2) can be accurately approximated by the projection matrix **V** in relation to a considerably reduced vector **z** of order *n*. In other words, the original state vector is represented by a linear combination of column vectors from the projection matrix **V**. Therefore, in this type of model reduction, the choice of the projection space **V** is very important. As the projection matrix, eigenvectors (Kim *et al.* 1986) and Ritz vectors (Wilson 1985) have been used in many engineering cases.

The Arnoldi process (Freund 2000, Bai 2002, Rudnyi *et al*. 2006) via implicit moment-matching is the most efficient way to compute a reasonably accurate subspace **V** for model reduction. Provided that the subspace **V** is found using this method, the original Eq. (2) is projected onto it. Multiplying the result by $\mathbf{V}^T$ yields the following reduced-order system:

$$\mathbf{M}_r \ddot{\mathbf{z}}(t) + \mathbf{C}_r \dot{\mathbf{z}}(t) + \mathbf{K}_r \mathbf{z}(t) = \mathbf{F}_r(t) \tag{12}$$

$$\mathbf{M}_r = \mathbf{V}^T \tilde{\mathbf{M}} \mathbf{V} \tag{13a}$$

$$\mathbf{C}_r = \mathbf{V}^T \tilde{\mathbf{C}} \mathbf{V} \tag{13b}$$

$$\mathbf{K}_r = \mathbf{V}^T \tilde{\mathbf{K}} \mathbf{V} \tag{13c}$$

$$\mathbf{F}_r = \mathbf{V}^T \mathbf{F} \tag{13d}$$

Here, we assume that the linear combination of the Krylov basis vectors obtained by considering only the undamped stationary rotor-bearing system constitutes a good approximation of the dynamic characteristics of the damped rotating rotor-bearing system.

In the case of the moment-matching method for a proportionally damped dynamic system, it can be shown that if the projection matrix **V** is chosen from a Krylov subspace of dimension *n* as defined in Eq. (14), the reduced-order system matches the first *n* moments of the full-order system (Eid *et al*. 2007, Han 2012).

$$\text{colspan}\{\mathbf{V}\} = \mathcal{K}_n(\mathbf{K}^{-1}\mathbf{M}, \mathbf{K}^{-1}\mathbf{F}) = \text{span}\{\mathbf{K}^{-1}\mathbf{F}, \cdots, (\mathbf{K}^{-1}\mathbf{M})^{n-1}\mathbf{K}^{-1}\mathbf{F}\} \tag{14}$$

In more detail, the Krylov subspace is a subspace spanned by the original $\mathbf{K}^{-1}\mathbf{F}$ and the vectors produced by consecutive multiplication of the matrix $\mathbf{K}^{-1}\mathbf{M}$ with this vector up to $n-1$ times. Its resulting vectors form the basis for an *n*-dimensional subspace. Because the direct computation of the vectors is numerically unstable because of round-off errors, the Arnoldi process is used to construct an orthonormal basis. Moreover, because of the iterative nature of the Arnoldi algorithm, a reduced-order model (ROM) of any dimension ranging from one to the reduced order specified by the user can be obtained (Rudnyi *et al*. 2006). Note that the reduction of the dimensions of the system to $n << N$ is achieved in Eq. (12), and therefore it is possible to efficiently compute the damped eigenvalue problem. Here, the QEP of the reduced-order system is efficiently solved in MATLAB (The MathWorks 2011).

2.3 Quadratic eigenvalue analysis by Krylov subspace-based MOR

It can be assumed that the responses of the free vibration of the reduced damped system in Eq. (12) have the forms

$$\mathbf{z}(t) = \hat{\boldsymbol{\psi}} e^{\hat{\lambda} t} \tag{15a}$$

$$\dot{\mathbf{z}}(t) = \hat{\lambda}\hat{\boldsymbol{\psi}} e^{\hat{\lambda} t} \tag{15b}$$

$$\ddot{\mathbf{z}}(t) = \hat{\lambda}^2\hat{\boldsymbol{\psi}} e^{\hat{\lambda} t} \tag{15c}$$

where $\hat{\boldsymbol{\psi}} \in \Re^n$ is the *n*-dimensional vector of the amplitudes, and $\hat{\lambda}$ is the complex frequency of the reduced-order system. Substituting Eq. (15) into Eq. (12) gives the following QEP of the reduced-order system:

$$(\hat{\lambda}^2\mathbf{M}_r + \hat{\lambda}\mathbf{C}_r + \mathbf{K}_r)\hat{\boldsymbol{\psi}} = \mathbf{0} \tag{16}$$

Using a 2*n*-dimensional vector **w** defined as

$$\mathbf{w} = \begin{Bmatrix} \mathbf{z} \\ \dot{\mathbf{z}} \end{Bmatrix} \tag{17}$$

the QEP in the displacement space is transformed into the state space in the same way as the previous full-order system, that is,

$$\underbrace{\begin{bmatrix}\mathbf{I}_n & \mathbf{0}\\ \mathbf{0} & \mathbf{M}_r\end{bmatrix}}_{\mathbf{E}_r}\underbrace{\begin{Bmatrix}\dot{\mathbf{z}}\\ \ddot{\mathbf{z}}\end{Bmatrix}}_{\dot{\mathbf{w}}}+\underbrace{\begin{bmatrix}\mathbf{0} & -\mathbf{I}_n\\ \mathbf{K}_r & \mathbf{C}_r\end{bmatrix}}_{\mathbf{A}_r}\underbrace{\begin{Bmatrix}\mathbf{z}\\ \dot{\mathbf{z}}\end{Bmatrix}}_{\mathbf{w}}=\mathbf{0} \tag{18}$$

Thus, the QEP of the reduced-order system given in Eq. (16) is transformed into the following 2*n*-dimensional first-order eigenvalue problem:

$$(\hat{\lambda}\mathbf{E}_r+\mathbf{A}_r)\hat{\boldsymbol{\eta}}=\mathbf{0} \tag{19}$$

in which

$$\hat{\boldsymbol{\eta}}=\begin{Bmatrix}\hat{\boldsymbol{\psi}}\\ \hat{\lambda}\hat{\boldsymbol{\psi}}\end{Bmatrix} \tag{20}$$

We expect that the complex eigenvalue λ_i is equal to $\hat{\lambda}_i$ and the eigenvector $\boldsymbol{\psi}_i$ is equal to $\mathbf{V}_n\hat{\boldsymbol{\psi}}_i$ for some order *k*, which is lower than the order of reduced system used for the projection (*n*), that is,

$$\lambda_i=\hat{\lambda}_i \tag{21a}$$

$$\boldsymbol{\psi}_i=\mathbf{V}_n\hat{\boldsymbol{\psi}}_i \quad \text{where} \quad i=1,\cdots,k<n \tag{21b}$$

It is necessary to note that in the suggested MOR for the QEP resulting from the Campbell diagram analysis, the generation of projection subspace **V** is independent of the rotational velocity, Ω, because the reduced-order matrices are given by

$$\mathbf{M}_r=\mathbf{V}^T\widetilde{\mathbf{M}}\mathbf{V} \tag{22a}$$

$$\mathbf{C}_r=\mathbf{V}^T\widetilde{\mathbf{C}}\mathbf{V}=\mathbf{V}^T(\mathbf{C}_S+\Omega\mathbf{G}_1)\mathbf{V}=\mathbf{V}^T\mathbf{C}_S\mathbf{V}+\Omega(\mathbf{V}^T\mathbf{G}_1\mathbf{V}) \tag{22b}$$

$$\mathbf{K}_r=\mathbf{V}^T\widetilde{\mathbf{K}}\mathbf{V} \tag{22c}$$

where $\mathbf{C}_S$ represents the structural damping matrix, and $\mathbf{G}_1$ is the gyroscopic matrix evaluated at Ω = 1 rad/s. In this case, the projection subspace is obtained from Eq. (14) using

$$\mathbf{F}=\begin{Bmatrix}1\\ \vdots\\ 1\end{Bmatrix}\in\Re^N \tag{23}$$

In this approach, because the generation of **V** is independent of the rotational velocity, it can be preserved as a parameter, and only one projection is necessary for each system matrix, irrespective of Ω. This results in better computational performance for the calculation of Campbell diagrams using ROMs.

3. Numerical examples

3.1 Turbomolecular pump

At present, the TMP is one of the most frequently used pumps to generate and maintain high and clean vacuum conditions in industry. Higher performance requires a higher rotational pumping speed; thus, in the TMP design currently used, rotordynamic problems such as those dealing with the critical speed are of increasing concern (Chiang *et al*. 2009). As shown in Fig. 1, the FE model for a TMP rotor system consists of a cylindrical rotor with eight-stage blades and a shaft supported by two sets of ball bearings (brgA and brgB in Fig. 1). The material used in the shaft is stainless steel; its Young's modulus, Poisson's ratio, and density are E = 193 GPa, ν = 0.31, and ρ = 7,450 kg/m^3, respectively. The rotor is made of an aluminum alloy (AL 2024-T6), and it has a Young's modulus E = 72.4 GPa, Poisson's ratio ν = 0.33, and density ρ = 2,780 kg/m^3. The stiffness coefficients of the isotropic brgA and brgB bearings used for QEP are $K_{XX} = K_{YY} = 40 \times 10^6$ N/m and $K_{XX} = K_{YY} = 20 \times 10^6$ N/m, respectively.

The blades have different shapes and sizes at each stage; they are replaced with a lumped mass element to construct the FE model. Table 1 lists the geometrical properties of the blades at each stage of the TMP rotor used for the FE model. The stages are numbered from top to bottom, as shown in Fig. 1. The FE model has 124,989 elements, and the total number of DOFs is up to 378,012.

A Campbell diagram analysis of the model is performed, as shown in Fig. 2. The Campbell diagram is evaluated with the full-order model (FOM) and an angular velocity up to 2,500 rad/s, which is the operational spin speed of the rotor system. For the plot of the diagram, QEP, as expressed in Eq. (5), is solved for ten different spin velocities. The intersection point between the first forward whirling frequency curve and the excitation line (1 × spin) indicates the critical speed of the TMP rotor system. Fig. 2 shows some whirling mode shapes of the TMP rotor system at the operational spin velocity.

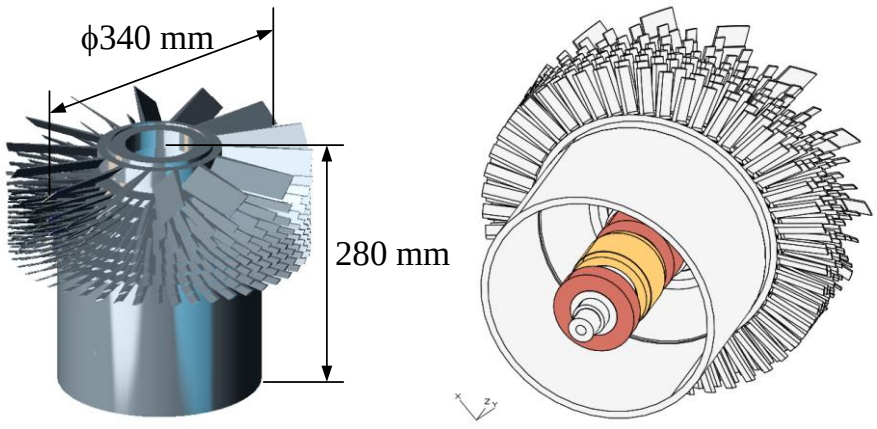

(a) CAD model

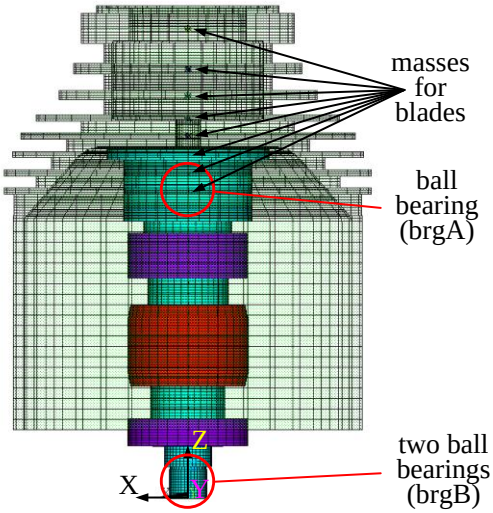

(b) Finite element model

Fig. 1 TMP rotor system

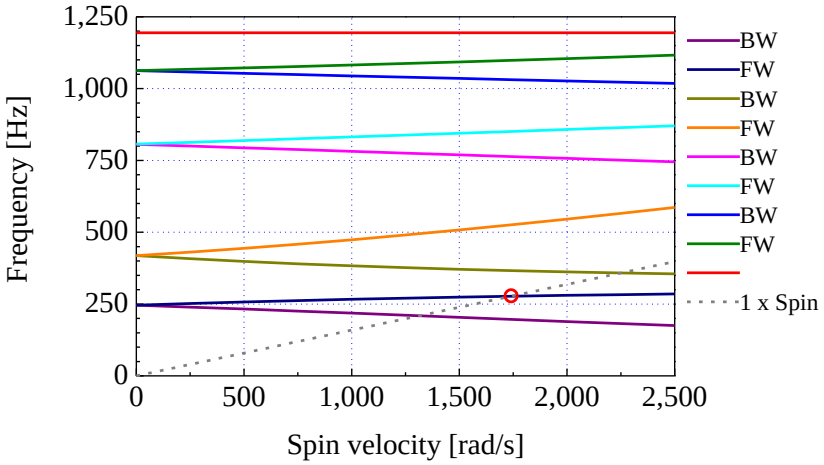

Fig. 2 Campbell diagram for the TMP rotor system

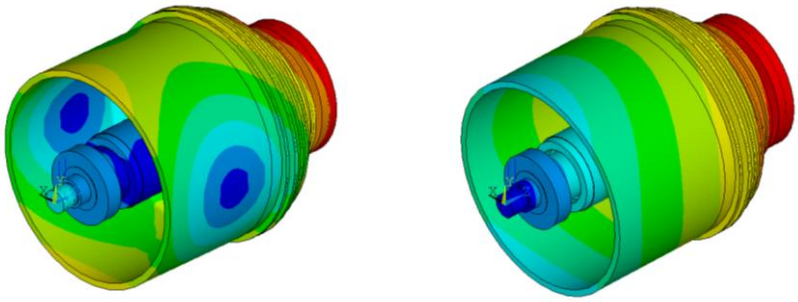

(a) First backward whirling (174.9 Hz) (b) First forward whirling (285.1 Hz)

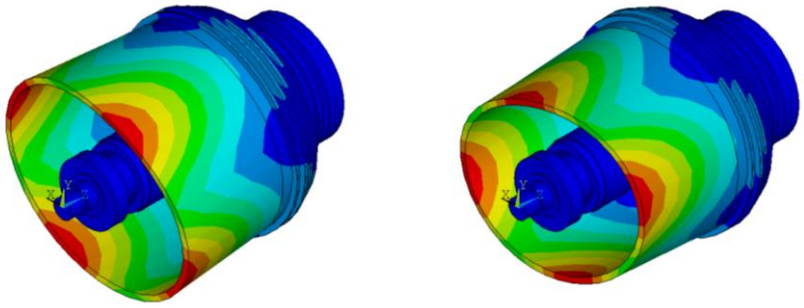

(c) Third backward whirling (745.1 Hz) (d) Third forward whirling (870.6 Hz)

Fig. 3 Whirling mode shapes of TMP rotor system

In terms of numerical accuracy, the damped frequencies between the FOM and ROMs are compared at three rotational velocities (see Tables 2–4). The percentage of relative error is calculated from the relation $100 \times (f_{ROM} - f_{FOM})/f_{FOM}$.

In this example, ROMs of order 40 and 50 are used to calculate the damped frequencies. Table 2 lists the damped frequencies for the case when the rotational velocity is 0 rad/s, i.e., no rotor spin. The frequencies approximated by the suggested method are extremely accurate. For instance, the ROM of order 40 gives the largest relative error, at about 0.007%. It should be noted that the ROM of order 40 seems to already have convergence up to the ninth mode. At the rotational velocity of 1,250 rad/s, the approximate damped frequencies are also very accurate (see Table 3). The ROM of order 40 gives the largest relative error about 0.03%. When the rotational velocity Ω = 2,500 rad/s, the approximate damped frequencies are also very close to those obtained in the FOM. In this case, the largest relative errors are about 0.17% for n = 40 and 0.14% for n = 50. It should be noted that higher-order ROMs have smaller relative errors and yield accurate damped frequencies up to higher modes than lower-order ROMs.

Table 1 The geometrical properties of the blades at each stage of the TMP rotor

Stage No.	Mass (kg)	Center of gravity	Mass moment of inertia		
		C. G. (mm)	I_{XX} (kg·mm^2)	I_{YY} (kg·mm^2)	I_{ZZ} (kg·mm^2)
1	0.363	308.8	2273.5	2273.5	4524.6
2	0.314	282.2	2145.2	2146.1	4287.9
3	0.306	264.9	2283.0	2283.0	4564.1
4	0.290	249.7	2580.6	2580.5	5160.2
5	0.205	238.4	2024.5	2025.0	4048.9
6	0.163	225.8	1667.2	1667.2	3334.0
7	0.134	213.6	1416.3	1416.3	2832.1
8	0.107	201.8	1129.2	1129.2	2258.1
Total	1.882	260.9	17515.0	17516.4	31010.0

Table 2 Comparison of damped frequency between FOM and ROMs (Ω = 0 rad/s)

Mode No.	Whirl	Damped frequency			Relative error (%)	
		FOM (N = 378,012)	ROM (n = 40)	ROM (n = 50)	ROM (n = 40)	ROM (n = 50)
1	BW	245.820	245.820	245.820	-0.0001	-0.0001
2	FW	245.820	245.820	245.820	0.0001	0.0001
3	BW	418.799	418.799	418.799	-0.0000	-0.0000
4	FW	418.801	418.801	418.801	-0.0001	-0.0001
5	BW	806.176	806.175	806.175	-0.0001	-0.0001
6	FW	806.789	806.788	806.788	-0.0001	-0.0001
7	BW	1062.452	1062.451	1062.451	-0.0001	-0.0001
8	FW	1062.471	1062.452	1062.452	-0.0018	-0.0018
9	-	1194.486	1194.401	1194.401	-0.0071	-0.0071

Table 3 Comparison of damped frequency between FOM and ROMs (Ω = 1,250 rad/s)

Mode No.	Whirl	Damped frequency			Relative error (%)	
		FOM (N = 378,012)	ROM (n = 40)	ROM (n = 50)	ROM (n = 40)	ROM (n = 50)
1	BW	210.967	210.998	210.993	0.0147	0.0121
2	FW	270.618	270.638	270.635	0.0074	0.0061
3	BW	376.544	376.589	376.580	0.0120	0.0096
4	FW	490.476	490.644	490.612	0.0342	0.0277
5	BW	775.423	775.668	775.668	0.0316	0.0316
6	FW	838.244	838.519	838.519	0.0328	0.0328
7	BW	1039.830	1039.928	1039.904	0.0094	0.0071
8	FW	1087.395	1087.521	1087.489	0.0116	0.0087
9	-	1194.394	1194.394	1194.394	0.0000	-0.0000

Table 4 Comparison of damped frequency between FOM and ROMs (Ω = 2,500 rad/s)

Mode No.	Whirl	Damped frequency			Relative error (%)	
		FOM (N = 378,012)	ROM (n = 40)	ROM (n = 50)	ROM (n = 40)	ROM (n = 50)
1	BW	174.918	175.010	174.993	0.0524	0.0429
2	FW	285.158	285.206	285.198	0.0167	0.0141
3	BW	354.919	355.005	354.987	0.0243	0.0191
4	FW	586.169	587.142	586.965	0.1661	0.1358
5	BW	745.152	746.078	746.078	0.1243	0.1243
6	FW	870.620	871.775	871.775	0.1327	0.1327
7	BW	1018.200	1018.568	1018.482	0.0362	0.0277
8	FW	1116.713	1117.349	1117.191	0.0569	0.0428
9	-	1194.371	1194.372	1194.372	0.0001	0.0001

Table 5 Computation times for the Campbell diagram analysis

Computation time (s)	FOM	ROM	
		n = 40	n = 50
Total DOF	378,012	40	50
Meshing in ANSYS	16	16	16
Quadratic eigenvalue analyses in ANSYS	4,633	-	-
Processing of the FULL files	-	79	79
Generation of Krylov vectors	-	1,036	1,062
Quadratic eigenvalue analyses in MATLAB	-	40	51
Total time	4,649	1,171	1,208

We have demonstrated the numerical accuracy of ROMs used to calculate approximate damped frequencies for a Campbell diagram analysis. Next, we compare the efficiencies of the computation times for calculating the damped frequencies. The calculations were performed using ANSYS and MATLAB on an HP workstation xw8400 with dual Xeon 5160 processors and 32 GB RAM.

In the case of the FOM, the quadratic eigenvalue analyses for the Campbell diagram were performed in ANSYS using the DAMP method because MATLAB crashed with a memory overflow. The calculation of the Campbell diagram using the FOM took about 4,649 s. On the other hand, ROMs of $n = 40$ and 50 had substantially less computational costs of 1,171 and 1,208 s, or, 25.1% and 25.9% of that of the FOM, respectively. For the ROMs, the total computation time included the processing of the assembled global matrix files (.FULL files in ANSYS) to extract system matrices, the process of generating Krylov vectors using the Arnoldi algorithm, and quadratic eigenvalue analyses in MATLAB. The use of ROMs seemed to be very efficient for performing the Campbell diagram analysis, although extra computations were necessary, such as for the preparation of system matrices, matrix factorization, and the generation of Krylov vectors.

3.2 Nelson and McVaugh rotor

The second numerical example is a Campbell diagram analysis of the rotor-bearing system studied by Nelson and McVaugh (Nelson *et al*. 1976) (see Fig. 4). The rotor system consists of a flexible rotor with one rigid disk supported by two orthotropic bearings. The Young's modulus, Poisson's ratio, and density of the shaft material are $E = 200$ GPa, $\nu = 0.3$, and $\rho = 7{,}850$ kg/m^3, respectively. The stiffness coefficients of the two identical orthotropic bearings are $K_{YY} = K_{ZZ} = 35.03 \times 10^6$ N/m and $K_{YZ} = K_{ZY} = -8.756 \times 10^6$ N/m. The rigid disk is modeled using a lumped element with a mass of 1.401 kg, a diametral moment of inertia $I_{YY} = I_{ZZ} = 13.6$ kg·mm^2, and a polar moment of inertia $I_{XX} = 2$ kg·mm^2. The FE model for the rotor system has 55,949 elements, and the total number of DOFs is up to 169,757.

Fig. 5 shows a Campbell diagram of the model evaluated using the FOM with an angular velocity of up to 10,000 rad/s, the operational spin speed of the system. To plot the diagram, the QEP expressed in Eq. (5) is solved for six different spin velocities. The intersection points between the forward whirling frequency curves and the excitation line indicate the critical speed of the rotor. Fig. 6 shows some whirling mode shapes of the rotor at the operational spin velocity.

The damped frequencies calculated from ROMs are compared to those obtained from the FOM in the case of four rotational velocities (see Tables 6–9). In this example, ROMs of order 25 and

30 are used to calculate the damped frequencies because these orders of ROMs are high enough to obtain accurate damped frequencies. Table 6 lists the damped frequencies for the case when the rotor does not spin. The approximate frequencies using an ROM of order 25 are very accurate, and the largest relative error is approximately 0.004%. This means that the ROM of order 25 seems to already converge up to the 10th mode. Table 7 lists the damped frequencies for the rotational velocity of 2,000 rad/s. The approximate damped frequencies show good agreement with those of the FOM. For instance, ROMs of order 25 and 30 give the largest relative errors of approximately 0.01% and 0.007%, respectively. At the rotational velocity of 6,000 rad/s, the approximate damped frequencies are also accurate (see Table 8). The ROMs of order 25 and 30 give the largest relative errors of approximately 0.07% and 0.04%, respectively. When the rotational velocity Ω = 10,000 rad/s, the approximate damped frequencies are still close to those of the FOM. In this case, the largest relative errors are approximately 0.17% for n = 25 and 0.1% for n = 30. From the above comparison, a significant improvement in the computational efficiency is observed for the Campbell diagram analysis using the Krylov-subspace based MOR, with minimal loss of accuracy. It should also be noted that higher-order ROMs generally yield more accurate damped frequencies for the highest mode than lower-order ROMs.

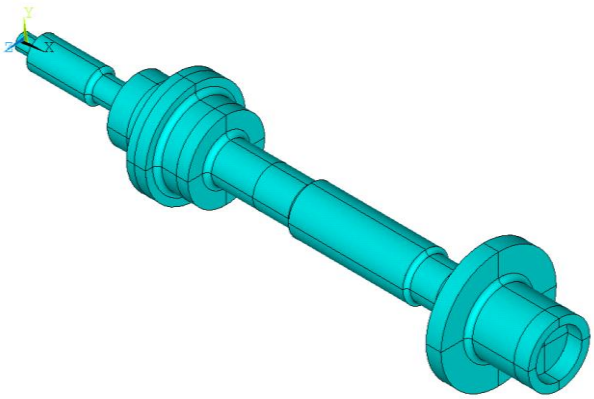

(a) CAD model

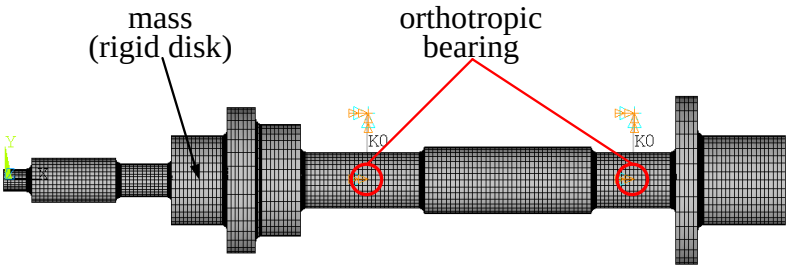

(b) Finite element model

Fig. 4 Nelson and McVaugh rotor

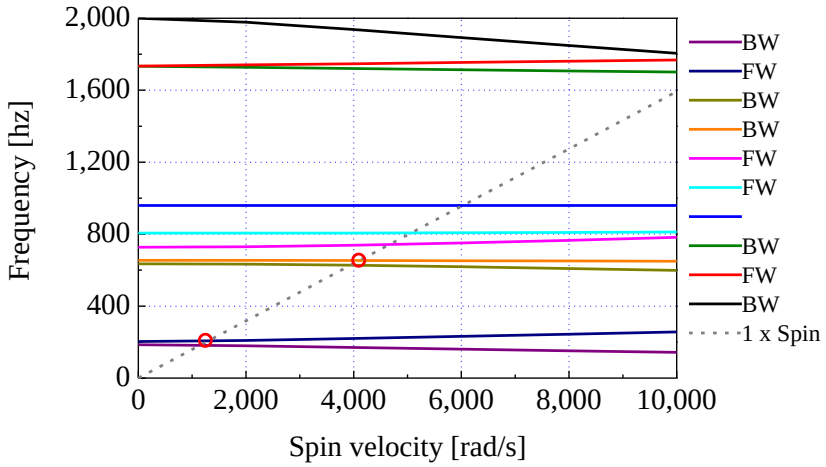

Fig. 5 Campbell diagram for the Nelson and McVaugh rotor

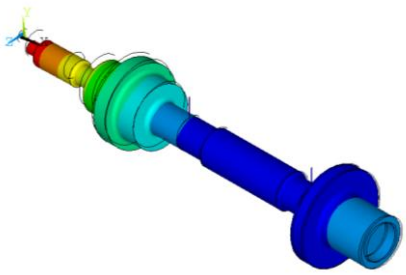

(a) First backward whirling (142.6 Hz)

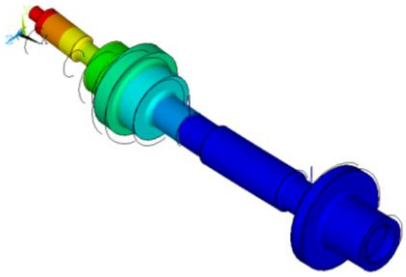

(b) First forward whirling (256.2 Hz)

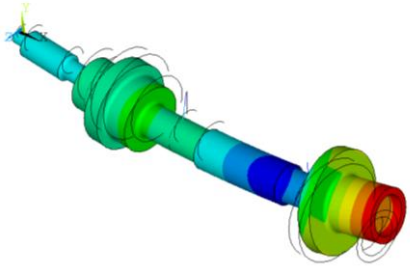

(c) Second backward whirling (598.5 Hz)

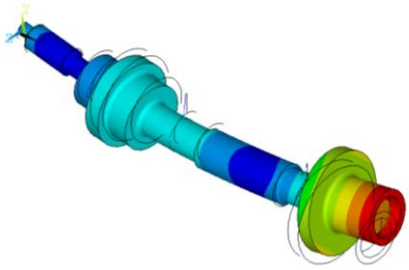

(d) Second forward whirling (781.9 Hz)

Fig. 6 Whirling mode shapes of Nelson and McVaugh rotor

Table 6 Comparison of damped frequency between FOM and ROMs (Ω = 0 rad/s)

Mode No.	Whirl	Damped frequency			Relative error (%)	
		FOM (N = 169,757)	ROM (n = 25)	ROM (n = 30)	ROM (n = 25)	ROM (n = 30)
1	BW	185.145	185.144	185.144	-0.0002	-0.0002
2	FW	203.636	203.636	203.636	-0.0001	-0.0001
3	BW	634.998	634.999	634.999	0.0002	0.0002
4	BW	654.837	654.850	654.850	0.0020	0.0020
5	FW	727.071	727.066	727.066	-0.0008	-0.0008
6	FW	805.690	805.679	805.679	-0.0014	-0.0014
7	-	959.530	959.530	959.530	-0.0000	-0.0000
8	BW	1733.581	1733.580	1733.580	-0.0001	-0.0001
9	FW	1733.999	1733.998	1733.998	-0.0000	-0.0000
10	BW	2000.409	2000.328	2000.328	-0.0041	-0.0041

Table 7 Comparison of damped frequency between FOM and ROMs (Ω = 2,000 rad/s)

Mode No.	Whirl	Damped frequency			Relative error (%)	
		FOM (N = 169,757)	ROM (n = 25)	ROM (n = 30)	ROM (n = 25)	ROM (n = 30)
1	BW	179.827	179.826	179.826	-0.0003	-0.0004
2	FW	209.397	209.398	209.398	0.0003	0.0003
3	BW	632.942	632.936	632.933	-0.0010	-0.0015
4	BW	654.434	654.442	654.441	0.0012	0.0010
5	FW	730.143	730.131	730.128	-0.0017	-0.0020
6	FW	805.838	805.881	805.880	0.0054	0.0053
7	-	959.530	959.530	959.530	0.0000	0.0000
8	BW	1727.130	1727.132	1727.132	0.0001	0.0001
9	FW	1740.493	1740.495	1740.495	0.0001	0.0001
10	BW	1977.952	1978.168	1978.099	0.0109	0.0074

Table 8 Comparison of damped frequency between FOM and ROMs (Ω = 6,000 rad/s)

Mode No.	Whirl	Damped frequency			Relative error (%)	
		FOM (N = 169,757)	ROM (n = 25)	ROM (n = 30)	ROM (n = 25)	ROM (n = 30)
1	BW	160.827	160.828	160.828	0.0011	0.0010
2	FW	231.831	231.834	231.834	0.0012	0.0012
3	BW	618.868	618.943	618.909	0.0121	0.0065
4	BW	652.354	652.386	652.377	0.0050	0.0035
5	FW	750.819	750.876	750.851	0.0076	0.0043
6	FW	807.523	807.565	807.553	0.0052	0.0037
7	-	959.529	959.529	959.529	0.0000	0.0000
8	BW	1713.921	1713.937	1713.937	0.0010	0.0010
9	FW	1754.056	1754.072	1754.072	0.0009	0.0009
10	BW	1892.842	1894.183	1893.681	0.0708	0.0444

Table 9 Comparison of damped frequency between FOM and ROMs (Ω = 10,000 rad/s)

Mode No.	Whirl	Damped frequency			Relative error (%)	
		FOM (N = 169,757)	ROM (n = 25)	ROM (n = 30)	ROM (n = 25)	ROM (n = 30)
1	BW	142.692	142.691	142.690	-0.0010	-0.0013
2	FW	256.293	256.294	256.294	0.0005	0.0004
3	BW	598.558	598.765	598.670	0.0346	0.0187
4	BW	649.681	649.753	649.733	0.0110	0.0080
5	FW	782.007	782.175	782.089	0.0214	0.0105
6	FW	811.772	811.854	811.833	0.0101	0.0076
7	-	959.528	959.527	959.527	0.0000	0.0000
8	BW	1700.690	1700.745	1700.742	0.0032	0.0031
9	FW	1767.867	1767.913	1767.912	0.0026	0.0025
10	BW	1805.330	1808.451	1807.257	0.1729	0.1067

Table 10 Comparison of damping exponent between FOM and ROMs (Ω = 10,000 rad/s)

Mode No.	Stability	Damping exponent			Relative error (%)	
		FOM (N = 169,757)	ROM (n = 25)	ROM (n = 30)	ROM (n = 25)	ROM (n = 30)
1	Stable	-1.430	-1.430	-1.430	0.0021	0.0019
2	Stable	-2.701	-2.700	-2.700	-0.0105	-0.0106
3	Stable	-21.102	-21.107	-21.106	0.0201	0.0179
4	Stable	-23.077	-23.077	-23.076	0.0001	-0.0017
5	Stable	-29.576	-29.563	-29.566	-0.0433	-0.0338
6	Stable	-34.846	-34.852	-34.850	0.0177	0.0119
7	Stable	-49.767	-49.767	-49.767	-0.0000	-0.0000
8	Stable	-159.408	-159.400	-159.401	-0.0053	-0.0045
9	Stable	-165.626	-165.623	-165.623	-0.0018	-0.0020
10	Stable	-196.834	-196.988	-196.929	0.0783	0.0484

Table 11 Computation times for the Campbell diagram analysis

Computation time (s)	FOM	ROM	
		n = 25	n = 30
Total DOF	169,757	25	30
Meshing in ANSYS	10	10	10
Processing of the FULL files	-	46	46
Generation of Krylov vectors	-	63	68
Quadratic eigenvalue analyses in MATLAB	5,880	15	17
Total time	5,890	134	141

In order to check the stability of each mode, the real parts of the eigenvalues need to be investigated. The real parts of the eigenvalues, σ_i, are called as the system damping exponents and a positive damping exponent indicates system instability in the linear sense. For simplicity, the

damping exponents for the rotational velocity of 10,000 rad/s are listed in Table 10. In this case, as a damping for the rotor system, Rayleigh damping with $\beta = 0.172$ μs is assumed to increase the magnitude of damping exponents because the undamped system has nearly zero damping exponent values. The approximate damping exponents calculated from ROMs maintain a level of accuracy similar to that of the FOM as the damped frequencies do. Generally, it has been reported for the moment matching methods that stability and passivity are not necessarily preserved in the resulting reduced-order model, so that usually post-processing is needed to realize these properties (Bai 2002). In this numerical example, the stability is preserved and the stability of each mode can be identified by the approximate complex eigenvalues using ROMs.

In terms of numerical efficiency, the computation times of the ROMs are compared with that of the FOM (see Table 11). In the case of the FOM, the quadratic eigenvalue analyses for the Campbell diagram were performed in MATLAB using the "eigs" command. The calculation of the Campbell diagram using the FOM took about 5,890 s. On the other hand, ROMs of $n = 25$ and 30 gave substantially reduced computational costs of 134 and 141 s, or, 2.3% and 2.4% of that of the FOM, respectively. The computational efficiency was higher than in the first example because a different solver for QEP was used for the FOM in this case. As previously mentioned, the FOM of the first example used the DAMP solver in ANSYS to calculate QEP.

A considerable time reduction is obtained in the computation of Campbell diagram analyses by using ROMs. The extra computation time needed to extract the system matrices and to generate Krylov vectors is minor compared to the quadratic eigenvalue analysis of the FOMs. Note that the computation times listed here may vary slightly, depending on the configuration and condition of S/W and H/W used for the calculation.

4. Conclusion

This study has demonstrated that reduced-order modeling using Krylov vectors can play an important role in reducing the numerical costs of a rotordynamic analysis. The MOR based on a Krylov subspace via moment matching significantly speeds up the Campbell diagram analysis used to investigate the critical speeds and stability of rotor-bearing systems. Specifically, the following conclusions can be drawn from this study.

(1) The basic assumption of the suggested MOR that the linear combination of the Krylov basis vectors obtained by considering only the undamped stationary rotor-bearing system constitutes a good approximation of the complex eigenvalues of the damped rotating rotor-bearing system was shown to be reasonable in the two illustrative examples. This approach allows a significant reduction in the computation time, while retaining the essential rotordynamic characteristics and necessitating no modification to the existing FE models.

(2) In the suggested MOR for the QEP resulting from a Campbell diagram analysis, the generation of projection matrix $\mathbf{V}$ is independent of the rotational velocity Ω. This approach is very efficient because it is possible to repeat the QEP simulation using the same reduced system by changing only the operating rotational velocity, which can be preserved as a parameter in the process of model reduction.

Therefore, large-scale rotordynamic FE models, which have the problem of high computational cost for Campbell diagram simulation because of the repeated quadratic eigenvalue analyses, can be efficiently handled using the suggested MOR. The suggested approach can also be applied to an unbalanced response analysis, which necessitates the calculation of frequency responses at

numerous frequencies of interest.

Acknowledgement

This research was supported by Energy Technology Development Program of Korea Institute of Energy Technology Evaluation and Planning (KETEP) grant funded by the Korea government's Ministry of Knowledge Economy (2012101010001C).

References

ANSYS, Inc. (2011), *ANSYS mechanical APDL Rotordynamic Analysis Guide, ANSYS Release 14.0*, Canonsburg, USA.

Antoulas, A.C., Sorensen, D.C. and Gugercin, S. (2001), "A survey of model reduction methods for large-scale systems", *Contemporary Mathematics*, **280**, 193-219.

Bai, Z. (2002), "Krylov subspace techniques for reduced-order modeling of large-scale dynamical systems", *Applied Numerical Mathematics*, **43**, 9-44.

Casciati, S. and Faravelli, L. (2014), "Quantity vs. Quality in the Model Order Reduction (MOR) of a Linear System", *Smart Struct. Syst.*, **13**(1), 99-109.

Chiang, H.W.D., Kuan, C.P. and Li, H.L. (2009), "Turbomolecular pump rotor-bearing system analysis and testing", *J. Vac. Sci. Technol. A*, **27**(5), 1196-1203.

Craig, R.R. and Bampton, M.C. (1968), "Coupling of substructures for dynamics analysis", *AIAA Journal*, **6**, 1313-1319.

Das, A.S. and Dutt, J.K. (2008), "Reduced model of a rotor-shaft system using modified SEREP", *Mechanics Research Communications*, **35**(6), 398-407.

Eid, R., Salimbahrami, B., Lohmann, B., Rudnyi, E. and Korvink, J. (2007), "Parametric order reduction of proportionally damped second-order systems", *Sensors and Materials*, **19**(3), 149-164.

Freund, R.W. (2000), "Krylov-subspace methods for reduced-order modeling in circuit simulation", *J. Comput. Appl. Math.*, **123**, 395-421.

Glasgow, D.A. and Nelson, H.D. (1980), "Stability analysis of rotor-bearing systems using component mode synthesis", *Journal of Mechanical Design, Transactions of the ASME*, **102**(2), 352-359.

Gugercin, S and Antoulas, A.C. (2004), "A survey of model reduction by balanced truncation and some new results", *International Journal of Control*, 77(8), 748-766.

Guyader, J.L. (2009), "Characterization and reduction of dynamic models of vibrating systems with high modal density", *Journal of Sound and Vibration*, **328**(4-5), 488-506.

Guyan, R.J. (1965), "Reduction of stiffness and mass matrices", *AIAA Journal*, **3**, 380.

Han, J.S. (2012), "Efficient frequency response and its direct sensitivity analyses for large-size finite element models using Krylov subspace-based model order reduction", *Journal of Mechanical Science and Technology*, **26**(4), 1115-1126.

Han, J.S. (2013), "Calculation of design sensitivity for large-size transient dynamic problems using Krylov subspace-based model order reduction", *J. Mech. Sci. Tech.*, **27**(9), 2789-2800.

Khulief, Y.A. and Mohiuddin, M.A. (1997), "On the dynamic analysis of rotors using modal reduction", *Finite Elements in Analysis and Design*, **26**, 41-55.

Kim, Y.D. and Lee, C.W. (1986), "Finite element analysis of rotor bearing systems using a modal

transformation matrix", Journal of Sound and Vibration, **111**(3), 441-456.
Mohiuddin, M.A., Bettayeb, M. and Khulief, Y.A. (1998), "Dynamic analysis and reduced order modelling of flexible rotor-bearing systems", *Computers and Structures*, **69**(3), 349-359.
Moore, B.C. (1981), "Principal component analysis in linear systems-controllability observability and model reduction", *IEEE Transactions on Automatic Control*, **26**(1), 17-2.
Nelson, F.C. (2007), "Rotor dynamics without equations", *International Journal of Condition Monitoring and Diagnostic Engineering Management*, **10**(3), 2-10.
Nelson, H.D. and McVaugh, J.M. (1976), "The dynamics of rotor-bearing systems using finite elements", *Journal of Engineering for Industry*, **98**, 593-600.
Qu, Z. (2004), *Model Order Reduction Techniques*, Springer, New York, NY, USA.
Rouch, K.E. and Kao, J. S. (1980), "Dynamic reduction in rotor dynamics by the finite element method", Journal of Mechanical Design, Transactions of the ASME, **102**(2), 360-368.
Rudnyi, E. and Korvink, J. (2006), "Model order reduction for large scale engineering models developed in ANSYS", *Lecture Notes in Computer Science*, **3732**, 349-356.
Sawicki, J.T. and Gawronski, W.K. (1997), "Balanced model reduction and control of rotor-bearing systems", *Journal of Engineering for Gas Turbines and Power*, **119**(2), 456-463.
Shanmugam, A. and Padmanabhan, C. (2006), "A fixed-free interface component mode synthesis method for rotordynamic analysis", Journal of Sound and Vibration, **297**(3-5), 664-679.
The MathWorks, Inc. (2011), *MATLAB Getting Started Guide*, Natick, USA.
Wagner, M.B., Younan, A., Allaire, P. and Cogill, R. (2010), "Model reduction methods for rotor dynamic analysis: a survey and review", *International Journal of Rotating Machinery*, **2010**, 1-17.
Wang, W. and Kirkhope, J. (1994a), "New eigensolutions and modal analysis for gyroscopic/rotor systems - part 1: undamped systems", *Journal of Sound and Vibration*, **175**(2), 159-170.
Wang, W. and Kirkhope, J. (1994b), "Component mode synthesis for damped rotor systems with hybrid interfaces", *Journal of Sound and Vibration*, **177**(3), 393-410.
Wang, W. and Kirkhope, J. (1995), "Complex component mode synthesis for damped systems", *Journal of Sound and Vibration*, **181**(5), 781-800.
Wang, G., Sreeram, V. and Liu, W.Q. (1999), "A new frequency weighted balanced truncation method and an error bound", *IEEE Transactions on Automatic Control*, **44**(9), 1734-1737.
Wilson, E.L. (1985), "A new method of dynamic analysis for linear and nonlinear systems", *Finite Elements in Analysis and Design*, **1**, 21-23.